

Dynamic bubble templating: What role does it play in the formation of corrosion products in iron drinking water pipes?

Tammie L. Gerke^a, Kirk G. Scheckel^b, Ricky I. Ray^c, and Brenda J. Little^c

^aDepartment of Geology, University of Cincinnati, Cincinnati, OH, 45221 USA,

Tammie.Gerke@uc.edu

^bU.S. Environmental Protection Agency, ORD, NRMRL, LRPCD 26 W. Martin Luther King Dr., Cincinnati, OH, 45268 USA, Scheckel.Kirk@epa.gov

^cNaval Research Laboratory, Stennis Space Center, MS 39529 USA,

Ricky.Ray@nrlssc.navy.mil, Brenda.Little@nrlssc.navy.mil

Abstract

Dynamic templating due to cathodic gas production is suggested as the mechanism for the formation of tube-like corrosion products on an unlined cast iron pipe in a drinking water distribution system. Mounds of corrosion product, mounds with protruding tubes and freestanding tubes were observed within a single 30 cm section of piping. Internal morphologies for all shapes were texturally complex although mineralogically simple, composed of two iron oxide/oxyhydroxides minerals: α -FeOOH (goethite) and Fe₃O₄ (magnetite).

Keywords: iron, μ -X-ray diffraction, μ -X-ray fluorescence mapping, tube shaped corrosion, morphologies.

1. Introduction

Unlined cast iron pipes (carbon, 2.1-4 wt%; silicon, 1.0-3.0 wt%; iron, balance), common in drinking water distribution systems (DWDS) worldwide, are highly susceptible to general (interchangeable anodes and cathodes) and localized corrosion (fixed anodes) with accumulations of iron corrosion products [1-3]. The predominant corrosion product morphology is mound-shape however other morphologies including flutes or cones, mounds with protruding tubes, and free standing tubes have been observed [4].

Research on the physicochemical characteristics and mechanism(s) of formation and growth have focused on mounds because of their prevalence. The internal structure of corrosion product mounds consists of a core, shell and surface layers [4]. Veinlets of Fe₃O₄ (magnetite) within core regions have also been reported [4-6]. Mechanisms of formation and growth are reasoned to be a result of iron release at the anode, followed by precipitation in close proximity to the anode [3]. Some mechanisms for mound formation indicate a spatial relationship between anodic sites and mound formation and a connection between the height of the mound and the depth of the resulting pit [7-9]. That relationship is not always obvious in DWDS where mounds can accumulate at locations with little evidence of pit formation [6]. Smith and

McEnaney [10] indicate corrosion product build-up as a result of both pitting and general corrosion.

Tube-shaped features are common in natural, quiescent environments, ranging in size from a few millimeters (soda straws in caves) to meters (chimneys at hydrothermal vents) [11], and form as a result of static and dynamic templating. Static templating is a process where precipitating material accumulates on an artificial or natural substrate whose shape controls the morphology of the precipitating material. Formation and growth of a tube on a dynamic template is not common and requires a constant and fairly uniform feature for precipitating material.

Baylis [12] proposed that flutes or cones formed in a manner similar to mounds but as the iron precipitated the corrosion product was elongated in the direction of water flow. Formation of tube-shaped iron corrosion products has been linked to the water calcium saturation index but no explanation regarding this relationship has been provided and no physicochemical characterization of the flutes/cones or tubes was presented [12].

In the following study, comprehensive physicochemical data were examined to evaluate the possibility of static and dynamic templating processes for creating tube-shaped iron corrosion products in DWDS. Samples were examined using traditional powder X-ray diffraction (XRD) and X-ray fluorescence (XRF) and synchrotron-based μ -XRD and μ -XRF mapping.

2. Experimental Design

2.1. Sample selection and preparation

An unlined cast iron DWDS pipe section (approximately 30 cm long by 15 cm inner diameter) containing mounds, mounds with protruding tubes and free standing tubes, was obtained from a drinking water utility in northeastern United States (Fig. 1). The pipe was cut in half and bulk samples were taken from one half of the pipe surface. Colors of the iron phases were determined according to Cornell and Schwartmann [13]. Samples were processed for bulk powder X-ray diffraction (XRD) and X-ray fluorescence (XRF) following the protocol of Gerke et al. [14].

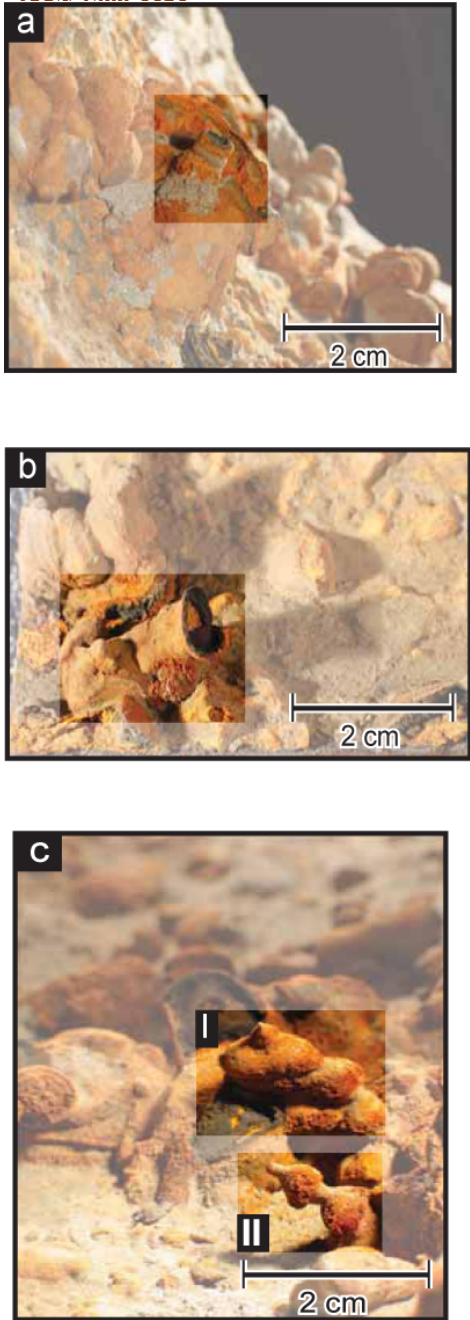


Fig. 1. Digital images of representative external morphologies of representative tube shaped iron corrosion products.

The other half of the pipe was encased in Buehler Epo Thin® Low Viscosity Epoxy and four representative samples of tubes and mounds with protruding tubes were harvested and digitally imaged. Sections were mounted on quartz slides, cut, and polished to an average thickness of 35 micrometers (Fig. 2). A mound and tube from the same sample (Fig. 2d) were used for synchrotron-based μ -XRD and μ -XRF mapping techniques.

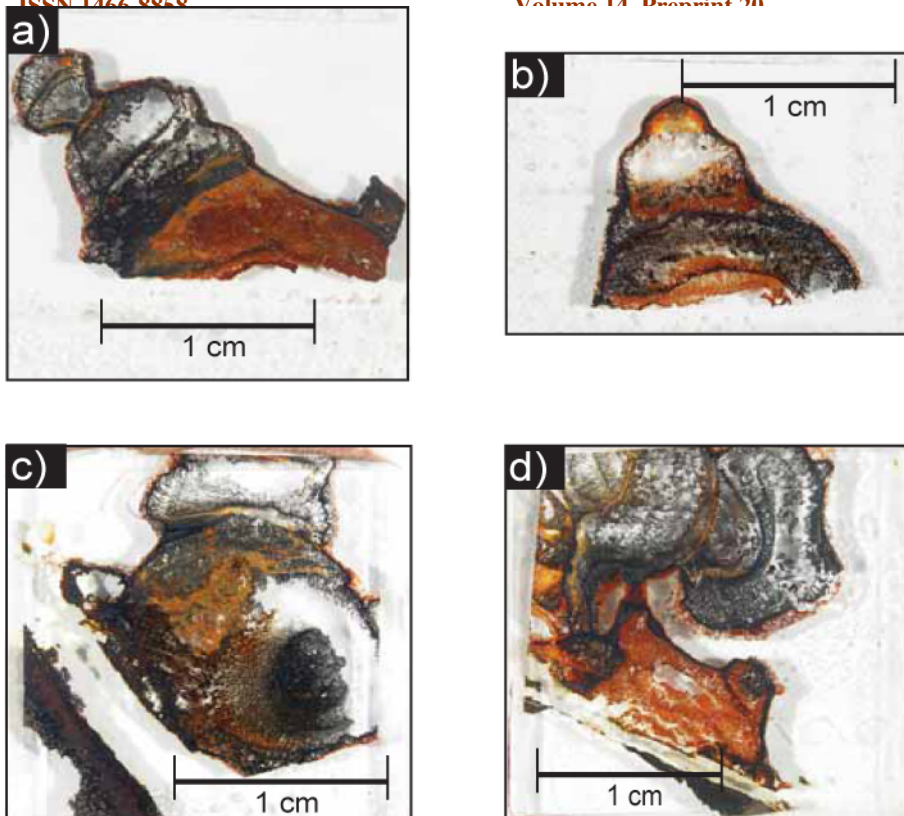


Fig. 2a-d. Internal morphologies cut: parallel to the long axis of a tube forming on a classical mound-shaped (a), parallel to the long axis of a free standing tube (T2) (b), perpendicular to the long axis of a tube (c) and a larger classical mound shaped with an associated large tube, and a smaller classical mound and tube shaped iron corrosion product (d).

2.2. Bulk sample analytical methods

Powder XRD diffraction and XRF analyses of the surface, shell, and core regions from a 5 cm sized mound-shaped iron corrosion product were conducted using the procedure of Gerke et al [14]. The iron pipe was examined using environmental scanning electron microscopy (ESEM) coupled with energy dispersive x-ray spectrometry (EDS) [15]. ESEM/EDS was used to determine the composition of the unlined iron pipe in two locations - under both a mound and a tube.

X-ray μ -beam studies (fluorescence and diffraction spectroscopies) were performed at XOR/PNC 20 BM-B of the Advanced Photon Source, Argonne National Laboratory (Argonne, IL) under standard operating conditions (7 GeV operation and ring current of 101 mA in top-up mode). Digital images of the representative mound and tube (Fig. 2d) were used to determine the locations for μ -XRF elemental maps and corresponding μ -XRD analyses. μ -XRF maps were recorded for Ca (calcium), Cr (chromium), Cu (copper), Fe (iron), Mn (manganese), Ni (nickel), and Zn (zinc). Relative elemental concentrations are shown using a color scale in which dark blue represents low concentrations and red represents comparatively higher concentrations. A MAR 165 charge-coupled detector was used for microcrystallography (μ -XRD) studies and points of interest were chosen based on location within the iron corrosion product and color. The

MAR 165 was positioned at approximately 200 mm from the sample and two dimensional μ -XRD patterns were collected for 300 s at 15 kV with a wavelength of 0.8265 Å. Two-dimensional diffractograms (2D Debye Scherrer rings) were converted to one-dimensional 2 θ scans using the software package Fit2D [16].

3. Results

3.1. Physicochemical characteristics of a representative five cm sized mound

The internal structure of mounds consisted of a core dominated by yellowish-red brown material, primarily α -FeOOH (goethite) with moderate amounts of metallic luster Fe_3O_4 (magnetite), and trace amounts of $CaCO_3$ (calcite) (Table 1). In addition the core was marbled with veinlets of black non-metallic luster Fe_3O_4 , minor amounts of α -FeOOH and trace amounts of $CaCO_3$ (Table 1). The uppermost portion of the core consisted of a thick layer of black non-metallic luster Fe_3O_4 , covered by a discontinuous shell-like layer composed of black Fe_3O_4 with a metallic luster and moderate amounts of $CaCO_3$ and trace amounts of α -FeOOH (Table 1). A discontinuous yellowish-red surface layer consisted of moderate amounts of γ -FeOOH (lepidocrocite), Fe_3O_4 , $CaCO_3$ and trace amounts of α -FeOOH, SiO_2 (quartz) and S (sulfur) (Table 1).

Iron concentrations were highest and Mn and Ca lowest in the core and associated veinlets (Table 2). The shell-like layer had the highest Ca concentrations, and the surface layer has the highest Pb, Mn, and Zn but the lowest Cu concentrations (Table 2). Ni and Cr concentrations were below detection for all regions (Table 2).

Table 1. Bulk powder X-ray diffraction and in-situ μ -X-ray diffraction identification of phases from iron corrosion products. Numbers in parentheses indicate location of analysis in Figs. 3 and 4.

Sample ID	Region of ICP ^a	α -FeOOH	γ -FeOOH	Fe_3O_4	CaCO_3	Accessory Minerals
5 cm size mound						
	surface	Trace	Moderate	Moderate	Moderate	SiO_2 or S
	shell	Trace	-	Dominant	Moderate	
	veinlets	Minor	-	Dominant	Trace	
	core	Dominant	-	Moderate	Trace	
0.25 cm sized mound						
	shell	?	-	Dominant	-	
	core (2)	Dominant	-	-	-	
	core (3)	Dominant	-	-	-	
	shell (4)	Moderate	-	Dominant	-	
0.50 cm sized tube						
	shell (1)	Minor/Trace	-	Dominant	-	
	core (2)	Dominant	-	Minor/Trace	-	
	core (3)	Minor/Trace	-	Dominant	-	
	core (4)	Minor/Trace	-	Dominant	-	
	core (5)	Minor/Trace	-	Dominant	-	
	core (6)	Dominant	-	Dominant	-	
	shell (7)	Minor	-	Dominant	-	

^a Iron corrosion product

Table 2. X-ray fluorescence elements, total carbon, and total sulfur data (w%) for regions of the macro-sized mound shaped iron corrosion product.

Region of ICP ^a	Fe	Mn	Ca	Pb	Zn	Cu	Ni	Cr
	%			$\mu\text{g kg}^{-1}$				
Surface	63.0	0.45	7.62	68	173	36	bd ^b	bd
Shell	66.4	0.10	11.31	17	39	52	bd	bd
Veinlets	85.4	0.04	1.21	22	36	51	bd	bd
Core	85.7	0.02	0.36	12	32	52	bd	bd

^a Iron corrosion product, ^b Below detection

3.2. Characteristics of one cm sized and smaller freestanding tubes and mounds with protruding tubes

A tube protruding from a mound (cut parallel to its long axis) had its base on what appeared to be a remnant surface layer (Fig. 2a). The upper portion of the tube constricted (tapered) and then broadened before closing completely. The tube consisted primarily of black non-metallic luster filamentous textured material separated into distinct zones by parallel layers of dense metallic luster black material. Two layers enclosed the entire iron corrosion product: a very thin black metallic luster layer of material overlain by a filamentous reddish-brown and non-metallic luster black material.

A freestanding tube (cut parallel to long axis) was composed of four packages of core and shell-like layers, vertically stacked on top of each other (Fig. 2b). A thick shell-like layer of black material enclosed the layers with a metallic luster overlain by a surface layer composed of red filamentous textured material.

The central region of a tube (cut perpendicular to long axis) was composed of dark brown to black non-metallic luster filamentous textured material (Fig. 2c). This material was enclosed by yellowish-brown to reddish-black, mostly filamentous textured material. A thin reddish-brown surface layer overlaid a thin shell-like layer composed of black, filamentous material with a metallic luster.

One of the most complex iron corrosion products, Fig. 2d, was a cm sized feature composed of two tubes and two mounds that appear to have grown together. A tube, on the left side of Fig. 2d, is composed almost entirely of black filamentous textured non-metallic luster material with bands of yellowish- to reddish-brown filamentous and black, metallic luster material. A mound-shaped structure, to the right of the tube, had a core of filamentous textured yellowish-red brown material. The smaller micro-sized mound- and tube-shaped iron corrosion products, located to the right of the mound-shaped structure, were examined in detail.

3.2.1. A 0.25 cm sized mound

The core of the mound (points 2 and 3, Fig. 3 C1) was composed of reddish-brown α -FeOOH. A shell-like layer of black metallic and non-metallic luster material (Fig. 3 HSL1) is composed

of Fe_3O_4 with moderate amounts of $\alpha\text{-FeOOH}$ at point 4 and possible trace amounts at point 1 and over lies the core. Covering the shell-like layer is a thin surface layer of filamentous textured reddish-brown material.

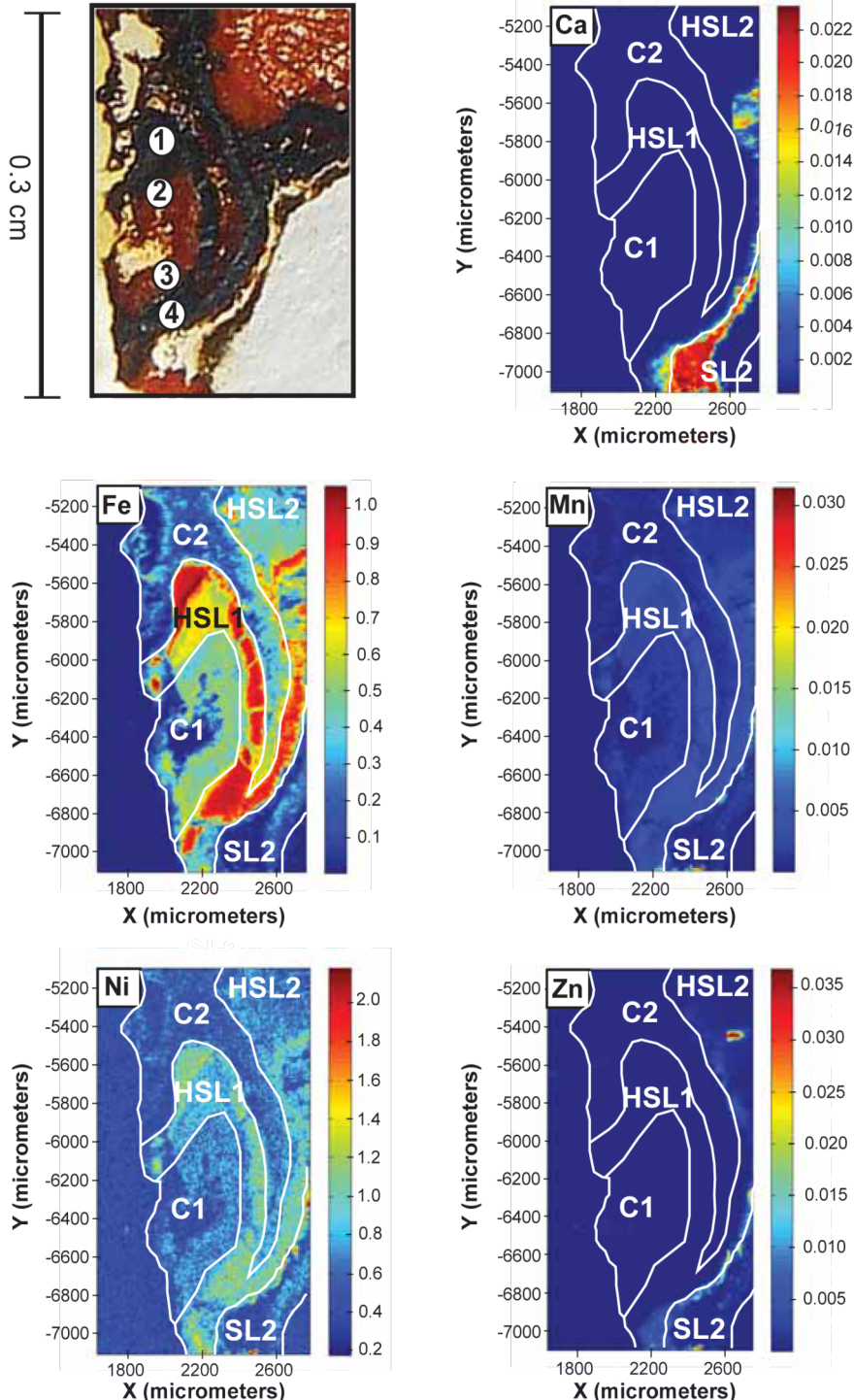


Fig. 3. μ -XRF maps of Ca, Fe, Mn, Ni, and Zn concentrations for a micro-sized classical mound shaped iron corrosion product. The numbers indicate the locations of the representative μ -XRD traces. C = core one, HSL = shell, SL = surface.

The fine scale distributions of Ca, Cr, Cu, Fe, Mn, Ni, and Zn were mapped using in-situ synchrotron μ -XRF (Fig. 3). Relative concentrations of Cr, Cu, and Zn were very low (data not presented) for all regions of the corrosion product. The lower (C1) and upper (C2) core region of the mound were composed primarily of Fe and trace amounts of Ni. The lower-most shell (HSL1) contained the highest concentration of Fe and moderate amounts of Ni. The outer shell (HSL2) had the same elemental distribution as S1. The surface material (SL1) was composed predominantly of Ca and contained lesser amounts of Fe and Ni.

3.2.2. A 0.25 cm sized tube

The micro-sized tube, oriented with its long axis perpendicular to the image, had an internal morphology similar to that in Fig. 2b), i.e., a central zone (CR1) of filamentous textured black material with a non-metallic luster, encircled by filamentous textured reddish- to yellowish-brown material (CR2) (Fig. 4). CR1 of the tube was composed primarily of Fe_3O_4 with minor to trace amounts of α -FeOOH (Fig. 4 points 3 – 5) and CR2 of α -FeOOH with minor to trace amounts of Fe_3O_4 (Fig. 4 points 2 and 6). All parts of this corrosion product were enclosed by a thin layer of metallic luster black Fe_3O_4 with minor to trace amounts of α -FeOOH (points 1 and 7; Fig. 4 HSL1). This is all overlain by a filamentous reddish-brown textured surface layer with some locations having black material with a non-metallic luster located at the outer edges.

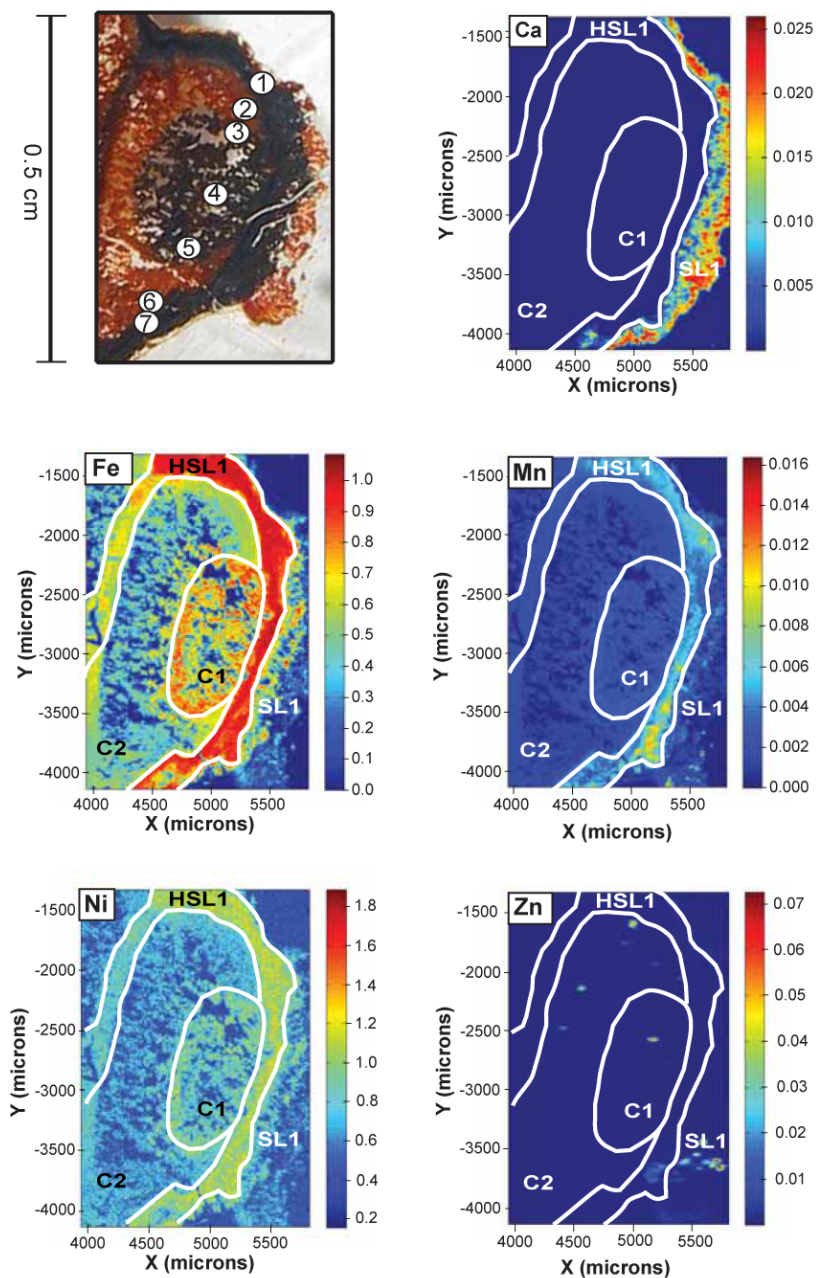


Fig. 4. μ -XRF maps of Ca, Fe, Mn, Ni, and Zn concentrations for a representative micro-sized tube shaped iron corrosion product. The numbers indicate the locations of the representative μ -XRD traces. C = core one, HSL = shell, SL = surface.

The in-situ synchrotron μ -XRF mapping of CR1 showed that it was composed of Fe, Ni and minor amounts of Mn (Fig. 4). Core region 2 (CR2) and the shell-like layer (HSL1) were also composed of Fe and lesser amounts of Ni and Mn. The surface material (SL1) was primarily composed of Ca with some Ni and Mn.

3.3. Pipe wall composition

The composition of the unlined cast iron pipe was qualitatively determined under the region of the 0.25 cm sized mound- and 0.50 cm sized tube-shaped iron corrosion products. The pipe was 74.54% iron and 18.75% silicon. Minor amounts of aluminum, phosphorus, chlorine, potassium, Mn, and Cu were detected. Additional regions of the pipe wall were analyzed and had very similar compositions (within the standard deviation of the EDS analysis; data not shown). All compositions were consistent with reported grey cast iron [17].

4. Discussion

Baylis [12] proposed a relationship between the calcite saturation index of water and the formation of tube-shaped corrosion products. In this work calcite was the main accessory phase associated with cm sized mounds and a discrete layer of calcium was associated with the smaller 0.25 cm sized mound- and 0.50 cm sized tube-shaped corrosion products, indicating that the corrosion products formed in water near or exceeding the calcite saturation index. Therefore at least for the pipe in this study there was no relationship between tube-shaped iron corrosion products and the calcite saturation index.

In DWDS the most likely static templates are minerals and microorganisms. Typical mineral phases associated with iron corrosion products include α - or γ -FeOOH and Fe_3O_4 and accessory phases such as $FeCO_3$ (siderite) and $CaCO_3$ [4,5,12,18-22]. In addition as metal ions from the pipe wall are released into the drinking water, they may form atypical, elongate mineral phases. Based on the pipe wall composition and the physicochemical analyses of the tube-shaped corrosion products no unique mineral phases were identified in this study. The general size of a single iron oxide/oxyhydroxide or calcite crystals in corrosion products is microns and none have elongate cylindrical morphology thus are not viable templating surfaces for producing cm sized features.

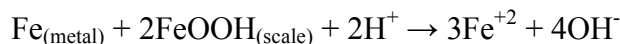
Microorganisms, present in all DWDS [23], can have rod-shaped morphologies or could produce filaments, sheaths or stalks which could produce static templates for tube-shaped features. For example, *Leptothrix ochracea* produces hollow sheaths (microtubes) that range in length from 10 to 200 μm and have an outer diameter of 1.4 μm [24]. ESEM analysis of corrosion products in this study though did not detect microorganisms or microbial features that could serve as templates. More importantly, static templating due to the presence of microorganisms produces structures that are orders of magnitude smaller than any of the tubes observed in the unlined cast iron pipe.

One potential mechanism for tube formation is precipitation of anodically produced iron particulate at cathodically produced gas bubbles. By physically separating the anode and cathode, Stone and Goldstein [25] generated tubular structures electrochemically in iron-ammonium sulfate solutions. The “ferrotubes” grew to millimeter size in tens to hundreds of minutes. In their work hydrogen gas bubbles were rapidly covered with precipitating iron creating a film that fractured and eventually slid onto the pipe surface creating the walls of a tube. They demonstrated that cathodic hydrogen gas production could provide the conditions for dynamic templating in a cast iron pipe. The iron oxides/hydroxides in the tube wall were arranged in the same oxidation sequence observed in the DWDS tubes.

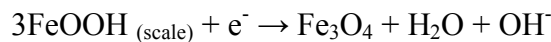
Butler and Ison [26] demonstrated that it was possible to form both tubes (hollow whiskers) and mound-shaped corrosion products in the same pipe during stagnation and high flow, respectively. Both conditions are common in residential mains, service lines and premise plumbing.

Regarding tube formation, Butler and Ison [26] proposed, “Ferrous ions, formed at the anodic area at the root of the whisker, diffuse along the tube, and growth of the whisker proceeds at the tip, where these ions are oxidized and precipitated as iron oxide on coming in contact with the aerated water.” Whiskers were up to 90 mm in length with growth rates more than 1mm per day. Whisker diameter tapered from 0.4 mm at the base to 0.2 mm at the growing tip. The whiskers were made up of goethite, magnetite and mixture of both.

As these authors [25,26] have demonstrated in laboratory experiments, the nature and location of the cathodic reaction can influence corrosion product morphology. Several cathodic reactions are possible in unlined cast iron pipes exposed to oxygenated, chlorinated drinking water. The most obvious potential cathodic reactions are reduction of water and O₂, resulting in H₂ and OH⁻, respectively. In the absence of oxygen it is possible for a previously deposited ferric scale to accept electrons as follows [27]:



McEnaney and Smith[27] suggested that under oxygen depleted conditions, FeOOH scale could be reduced to magnetite by a process of reductive dissolution as follows:



We suggest that this reaction can be used to explain the consistent mineralogy observed in mounds and tubes formed in oxygenated waters with differing chemistries [6].

Smith and McEnaney [10] observed chimney features that increased in numbers and length over time in corrosion products on grey cast iron in water at 50 °C and further observed that the chimneys were vents for corrosion products (including H₂) formed under the crust. They surmised that acidic conditions developed under the crust similarly to acidic regions near pits in chloride solutions of comparable concentrations (100 ppm Cl⁻) [29]. Mankowski and Szklarska-Smialowska [30] established that increased acidity within pits was a consequence of significant Cl⁻ levels above the bulk solution content. Smith and McEnaney[10] proposed that under acidic conditions H⁺ reduction (as opposed to water reduction in neutral conditions) would become the

cathodic process within the accumulated corrosion products and O₂ reduction would occur on the nodule crust. They did not relate growth of the chimneys to dynamic templating.

5. Conclusions

Comprehensive physicochemical data of corrosion products from mounds, mounds with protruding tubes and freestanding tubes were examined in detail and used to rationalize a proposed mechanism of formation. Regardless of form or size the physicochemical characteristics for all corrosion products were similar. The size of the tubes is inconsistent with static templating due to surface-bound microorganisms or mineral phases. Similarly, minerals were eliminated as static templates for tube formation. Dynamic templating because of cathodic hydrogen production is suggested as the mechanism for tube-like corrosion product formation in unlined cast iron piping.

In summary, we propose that in cast iron pipes exposed to aerated, chlorinated drinking water, metallic iron is oxidized to Fe⁺² by dissolved oxygen in the water, released into the water and further oxidized to Fe⁺³, forming Fe(OH)₃, which accumulates on the inner wall of the cast iron pipe at locations that are not necessarily associated with localized corrosion. The Fe(OH)₃ dehydrates and becomes FeOOH. Below a critical O₂ concentration FeOOH is reduced to Fe₃O₄. Gas production at the cathode causes breaks (vents) in the crust. Growth of the vents into tubes is the result of templating on the cathodically produced gas bubbles.

6. Acknowledgements

PNC/XOR facilities at the Advanced Photon Source, and research at these facilities, are supported by the US Department of Energy - Basic Energy Sciences, a major facilities access grant from NSERC, the University of Washington, Simon Fraser University and the Advanced Photon Source. Use of the Advanced Photon Source, an Office of Science User Facility operated for the U.S. Department of Energy (DOE) Office of Science by Argonne National Laboratory, was supported by the U.S. DOE under Contract No. DE-AC02-06CH11357. We would like to thank S. A. Walley and J. B. Maynard for their insightful comments on earlier versions of this paper and M. K. DeSantis for providing the digital images of the iron corrosion products. The opinions expressed in this paper are those of the author(s), and do not necessarily reflect the official positions and policies of the USEPA. Any mention of product or trade names does not constitute recommendation for use by the USEPA.

7. References

- [1] 'Study of corrosion material accumulated on the inner wall of steel water pipe', J. Lin and M. Ellaway, R. Adrien, *Corrosion Science*, **43**, 11, pp2065-2081, 2001.
- [2] 'Iron pipe corrosion in distribution systems', L.S. McNeill and M. Edwards, *Journal of American Water Works Association*, **93**, 7, pp.88-100, 2001.

- [3] 'Iron Corrosion Scales: Model for Scale Growth, Iron Release and Colored Water Formation', P. Sarin, V.L. Snoeyink, D.A. Lytle, W.M. Kriven, *Journal of Environmental Engineering*, **130**, pp364-373 (2004).
- [4] 'Prevention of Corrosion and Red Water', J.R. Baylis, *Journal of American Water Works Association*, **15**, 598-633, (1926).
- [5] 'Physio-chemical Characterization of Five Iron Tuberles from a Single Drkinking Water Distribution System: Possible New Insights on Their Formation and Growth', T.L. Gerke, J.B. Maynard, M.R. Schock, D.A. Lytle, *Corrosion Science*, **50**, 7, pp2030-2039, 2008.
- [6] 'The anatomy of tubercles: A corrosion study in a fresh water estuary', R. Ray, J. Lee, B. Little, T. Gerke, *Materials and Corrosion*, **61**, 12, pp993-999, 2010.
- [7] 'MIC Mythes - Does Pitting Cause MIC?', H. M. Herro, presented at *CORROSION*, Paper 278, San Diego, CA, 1998.
- [8] 'Predictive Model for Non-Microbially Influenced Corrosion Tuberculation', P. Angell, Final Report EPRI Palo Alto, California, 2003.
- [9] The NALCO Guide to Cooling Water System Failure Analysis. H.M. Herro, R.D. Port, McGraw-Hill, 1993.
- [10] 'The influence of dissolved oxygen concentration on the corrosoin of grey cast iron in water at 50°C', D.C. Smith, B. McEnaney, *Corrosion Science*, **19**, 6, pp379-394, 1979.
- [11] 'Submarine thermal springs on the Galápagos Rift', Corliss, J.B., Dymond, J., Gordon,L., Edmond, J.M., Herzen, R.P. Von., Ballard, R.D., Green, K., Bainbridge, A. Crane, K. and van Andel, T.H., *Science*, **203**, pp1073-1083, 1979.
- [12] 'Cast-Iron Pipe Coatings and Corrosion', J.R. Baylis, *Journal of American Water Works Association*, **45**, pp807-83, 1953.
- [13] The Iron Oxides; Structure, Properties, Reactions, Occurrences and Uses, R.M. Cornell, U. Schwertmann, Wiley-VCH Verlag GmbH & Co. KGaA, Darmstadt, 2003.
- [14] 'Speciation and distribution of vanadium in drinking water iron pipe corrosion by-products', T.L. Gerke, K.G. Scheckel, J.B. Maynard, *Science of the Total Environment*, **408**, pp5845-5853, 2010.
- [15] 'Environmental electron microscopy applied to Biofilms', In. Biofilms in Medicine, Industry and Environmental Biotechnology, R. Ray and B.J. Little Edited by Piet Lens, A.P. Moran, T. Mahony, P. Stoodley and V. O'Flaherty. IWA Publishing, London. pp331-351, 2003.

- [16] 'FIT2D: A Multi-Purpose Data Analysis and Display Program', A. Hammersley, *ESRF*, **10**, pp , 2001.
- [17] Troubleshooting Manufacturing Processes: Adapted from the Tool and Manufacturing Engineers Handbook, L.K. Gillespie, Society of Manufacturing Engineers, 1988.
- [18] 'Iron release from corroded iron pipes in drinking water distribution systems: effect of dissolved oxygen', P. Sarin, V.L. Snoeyink, J. Bebee, K.K. Jim, M.A. Beckett, W.M. Kriven, J.A. Clement, *Water Research*, **38**, 5, pp1259-1269, 2004.
- [19] 'Physico-chemical characteristics of corrosion scales in old iron pipes', P. Sarin, V.L. Snoeyink, J. Bebee, W.M. Kriven, J.A. Clement, *Water Research*, **35**, 12, pp2961-2969, 2001.
- [20] 'Mechanism of corrosion of cast iron covered by aged corrosion products: Application of electrochemical impedance spectrometry', M. Sancy, Y. Gourbeyre, E.M.M. Sutter, B. Tribollet, *Corrosion Science*, **52**, 4, pp1222-1227, 2010.
- [21] 'Characteristics of iron corrosion scales established under blending of ground, surface, and saline waters and their impacts on iron release in the pipe distribution system', Z. Tang, S. Hong, W. Xiao, J. Taylor, *Corrosion Science*, **48**, 2, pp322-342, 2006.
- [22] 'Effect of bacterial sulfate reduction on iron-corrosion scales', D.A. Lytle, T.L. Gerke, J.B. Maynard, *Journal of American Water Works Association*, **97**, 10, pp109-120, 2005.
- [23] 'Scanning electron microscope evidence for bacterial colonization of a drinking-water distribution system', H F Ridgway, and B H Olson, *Applied and Environmental Microbiology*. **41**, 1, pp274-287, 1981.
- [24] 'Characteristics of hollow microtubes consisting of amorphous iron oxide nanoparticles produced by iron oxidizing bacteria, Leptothrix ochracea', H. Hashimoto, S. Yokoyama, H. Asaoka, Y. Kusano, Y. Ikeda, M. Seno, J. Takada, T. Fujii, M. Nakanishi, R. Murakami, *Journal of Magnetism and Magnetic Materials*, **310**, pp2405-2407, 2007.
- [25] 'Tubular precipitation and redox gradients on a bubbling template', D.A. Stone, R.E. Goldstein, *Proceedings of the National Academy of Sciences of the United States of America*, **101**, 32, pp11537-11541, 2004.
- [26] 'An unusual form of corrosion product', G. Butler, H.C.K. Ison, *Nature*, **182**, 4644, pp1229-1230, 1958.
- [27] 'Investigations of the Reduction and Re-oxidation Kinetics of Iron (III) Oxide Scales Formed in Waters', A. Kuch, *Corrosion Science*, **28**, 3, pp221-231, 1988.
- [28] 'The reductive dissolution of FeOOH in Corrosion Scales Formed on cast Iron in Near-Neutral Waters', B. McEnaney and D.C. Smith *Corrosion Science*, **20**, pp873-886, 1980.

[29] 'Some Important Aspects of Corrosion in Central Heating Systems', G. Butler, H.C.K. Ison, A.D. Mercer, *British Corrosion Journal*, **6**, 1, pp31-38, 1971.

[30] 'Studies on accumulation of chloride ions in pits growing during anodic polarization', J. Mankowski, Z. Szklarska-Smialowska *Corrosion Science* **15**, pp493-501, 1975.